



## OPEN ACCESS

## EDITED BY

Gaetano Santulli,  
Albert Einstein College of Medicine,  
United States

## REVIEWED BY

Bin Yi,  
Army Medical University, China  
Paraskevi Papadopoulou,  
American College of Greece, Greece

## \*CORRESPONDENCE

Jaques Reifman,  
✉ jaques.reifman.civ@health.mil

RECEIVED 25 October 2023

ACCEPTED 09 January 2024

PUBLISHED 25 January 2024

## CITATION

Jin X, Frock A, Nagaraja S, Wallqvist A and  
Reifman J (2024), AI algorithm for personalized  
resource allocation and treatment of  
hemorrhage casualties.  
*Front. Physiol.* 15:1327948.  
doi: 10.3389/fphys.2024.1327948

## COPYRIGHT

© 2024 Jin, Frock, Nagaraja, Wallqvist and  
Reifman. This is an open-access article  
distributed under the terms of the [Creative  
Commons Attribution License \(CC BY\)](#). The use,  
distribution or reproduction in other forums is  
permitted, provided the original author(s) and  
the copyright owner(s) are credited and that the  
original publication in this journal is cited, in  
accordance with accepted academic practice.  
No use, distribution or reproduction is  
permitted which does not comply with these  
terms.

# AI algorithm for personalized resource allocation and treatment of hemorrhage casualties

Xin Jin<sup>1,2</sup>, Andrew Frock<sup>1,2</sup>, Sridevi Nagaraja<sup>1,2</sup>, Anders Wallqvist<sup>1</sup>  
and Jaques Reifman<sup>1\*</sup>

<sup>1</sup>Department of Defense Biotechnology High Performance Computing Software Applications Institute, Telemedicine and Advanced Technology Research Center, United States Army Medical Research and Development Command, Fort Detrick, MD, United States, <sup>2</sup>The Henry M. Jackson Foundation for the Advancement of Military Medicine Inc., Bethesda, MD, United States

A deep neural network-based artificial intelligence (AI) model was assessed for its utility in predicting vital signs of hemorrhage patients and optimizing the management of fluid resuscitation in mass casualties. With the use of a cardio-respiratory computational model to generate synthetic data of hemorrhage casualties, an application was created where a limited data stream (the initial 10 min of vital-sign monitoring) could be used to predict the outcomes of different fluid resuscitation allocations 60 min into the future. The predicted outcomes were then used to select the optimal resuscitation allocation for various simulated mass-casualty scenarios. This allowed the assessment of the potential benefits of using an allocation method based on personalized predictions of future vital signs *versus* a static population-based method that only uses currently available vital-sign information. The theoretical benefits of this approach included up to 46% additional casualties restored to healthy vital signs and a 119% increase in fluid-utilization efficiency. Although the study is not immune from limitations associated with synthetic data under specific assumptions, the work demonstrated the potential for incorporating neural network-based AI technologies in hemorrhage detection and treatment. The simulated injury and treatment scenarios used delineated possible benefits and opportunities available for using AI in pre-hospital trauma care. The greatest benefit of this technology lies in its ability to provide personalized interventions that optimize clinical outcomes under resource-limited conditions, such as in civilian or military mass-casualty events, involving moderate and severe hemorrhage.

## KEYWORDS

artificial intelligence, fluid resuscitation, hemorrhage, resource utilization, trauma

## Introduction

Uncontrolled bleeding remains the major cause of preventable civilian and battlefield trauma deaths, with the greatest loss of life occurring in the pre-hospital environment (Eastridge et al., 2012; Kisat et al., 2013; Davis et al., 2014; Chang et al., 2016; Gurney and Spinella, 2018). The ability to identify and treat hemorrhage continues to be a top priority in combat casualty care, and attention is increasingly shifting toward conditions involving multiple casualties in austere and resource-constrained environments (Dolan et al., 2021; Lesperance et al., 2023). In these cases, artificial intelligence (AI) technologies represent a promising approach, providing decision support for triage, treatment, and resource

prioritization at the lowest echelons of care (Raita et al., 2019; Fernandes et al., 2020; Liu et al., 2023; Peng et al., 2023).

The U.S. Department of Defense (DoD) has established practical population-based guidelines, procedures, and protocols to help combat medics identify and treat trauma-induced hemorrhage and provide fluid resuscitation in accordance with signs and symptoms, such as those provided by the Vampire Program (Voller et al., 2021) and the Tactical Combat Casualty Care guidelines (Deaton et al., 2021). These protocols encode robust and tried procedures that optimize outcomes when resources are readily available. Although they are based on population studies and do not provide patient-specific recommendations, these guidelines represent state-of-the-art field care, designed to support trained medics.

Machine-learning methods have been proposed to support the automation of casualty treatment, such as closed-loop fluid resuscitation (Kramer et al., 2008; Rinehart et al., 2013; Marques et al., 2017; Jin et al., 2018; Gholami et al., 2021; Alsalti et al., 2022; Avital et al., 2022). Although these treatments can potentially optimize fluid resuscitation for one casualty at a time, they do not address the simultaneous management of multiple casualties under resource-constrained conditions. Similarly, for the unstructured pre-hospital and the structured hospital environments, machine-learning methods have been developed to predict the need for life-saving interventions (Liu et al., 2014), including massive blood transfusion (Mina et al., 2013; Hodgman et al., 2018; Lammers et al., 2022), and to automatically analyze vital-sign data and stratify hemorrhage risk in trauma casualties (Stallings et al., 2023). While these methods flag the need for treatment, they do not necessarily provide a personalized resuscitation plan for each individual casualty.

Arguably, the main factor limiting the development of data-driven AI solutions for field care and triage of hemorrhage injuries is the lack of well-annotated and curated data to train these algorithms. In particular, deep neural network approaches used in the most powerful applications, such as large language models in medicine (Walker et al., 2023), require depth and breadth of quality data to become reliable. Here, we addressed this problem by using synthetic data derived from our previously developed cardio-respiratory (CR) mathematical model (Jin et al., 2023) to simulate multiple moderate to severe hemorrhage and fluid resuscitation scenarios, which we used to develop a recurrent neural network model capable of predicting treatment outcomes for each casualty 60 min into the future based on just 10 min of vital-sign data as input to the AI model. We then contrasted a resource-allocation method that used the AI-predicted outcomes with the DoD's Vampire Program (Voller et al., 2021) to understand the prospective value and benefits of using such a method in mass-casualty scenarios and various resource-limited conditions. We hypothesized that we could use the neural network-based AI technologies in hemorrhage treatment to more efficiently allocate fluids to optimize clinical outcomes.

## Materials and methods

### Cardio-respiratory model

We used the CR model (Jin et al., 2023) to generate synthetic data that capture the time-dependent evolution of vital signs

associated with hemorrhage and subsequent fluid resuscitation treatments. The CR model integrates cardiovascular and respiratory processes with their regulatory mechanisms to provide physiologically appropriate vital-sign time-course data that mimic the human response to hemorrhage and related treatments. The model consists of 74 ordinary differential and algebraic equations with 74 parameters. The inputs to the model include the rate of hemorrhage, rate of fluid resuscitation, minute ventilation, and fraction of inspired oxygen; the model outputs consist of arterial blood pressure [systolic (SBP), diastolic, and mean], heart rate (HR), partial pressure of end-tidal carbon dioxide, and oxygen saturation.

The CR model utilizes a lumped-parameter formulation based on first principles (conservation of mass) to represent fluid balances within vascular compartments and gas balances within the lungs and tissues, as well as a compartmental phenomenological formulation to represent the regulatory mechanisms and couplings between the cardiovascular and respiratory modules. Through this framework, the CR model enables the simulation of hemorrhage, fluid resuscitation, and respiratory perturbations, facilitating the generation of synthetic data that simulate injury and treatment scenarios of interest. It is important to note that a current limitation of the CR model includes the inability to account for specific types of resuscitation fluids, as the model solely considers the volume of fluid administered. For a more comprehensive overview of the CR model's formulation and implementation, we direct the reader to Jin et al. (2023).

### Outline of the methodology to develop and assess the AI algorithm for personalized resource allocation of hemorrhage casualties

We performed the three steps depicted in Figure 1 to develop and assess the AI algorithm for personalized resource allocation of hemorrhage casualties.

- I) *Synthetic-data generation.* First, we performed simulations using the CR model to create synthetic vital-sign data and form a cohort of trauma casualties. The CR-model simulations generated vital-sign trajectories during an initial hemorrhage-inducing trauma, followed by four distinct fluid treatment options for each trauma casualty in the cohort. We considered this CR-generated synthetic data as the ground truth for subsequent analyses.
- II) *AI-model development.* To develop the AI model, we first divided the entirety of the CR-generated cohort of trauma casualties into five equally sized groups (20% each). Then, we performed a 5-fold nested cross-validation procedure in which we iteratively trained and validated the AI model on data from four groups, and tested the model's prediction performance on the data from the remaining fifth group. Through this process, we ensured that the AI model for each test group did not possess prior information regarding the vital signs of the casualties in that group. At the end of this iterative process, we obtained five AI models, one for each of the five groups, where we had trained the models

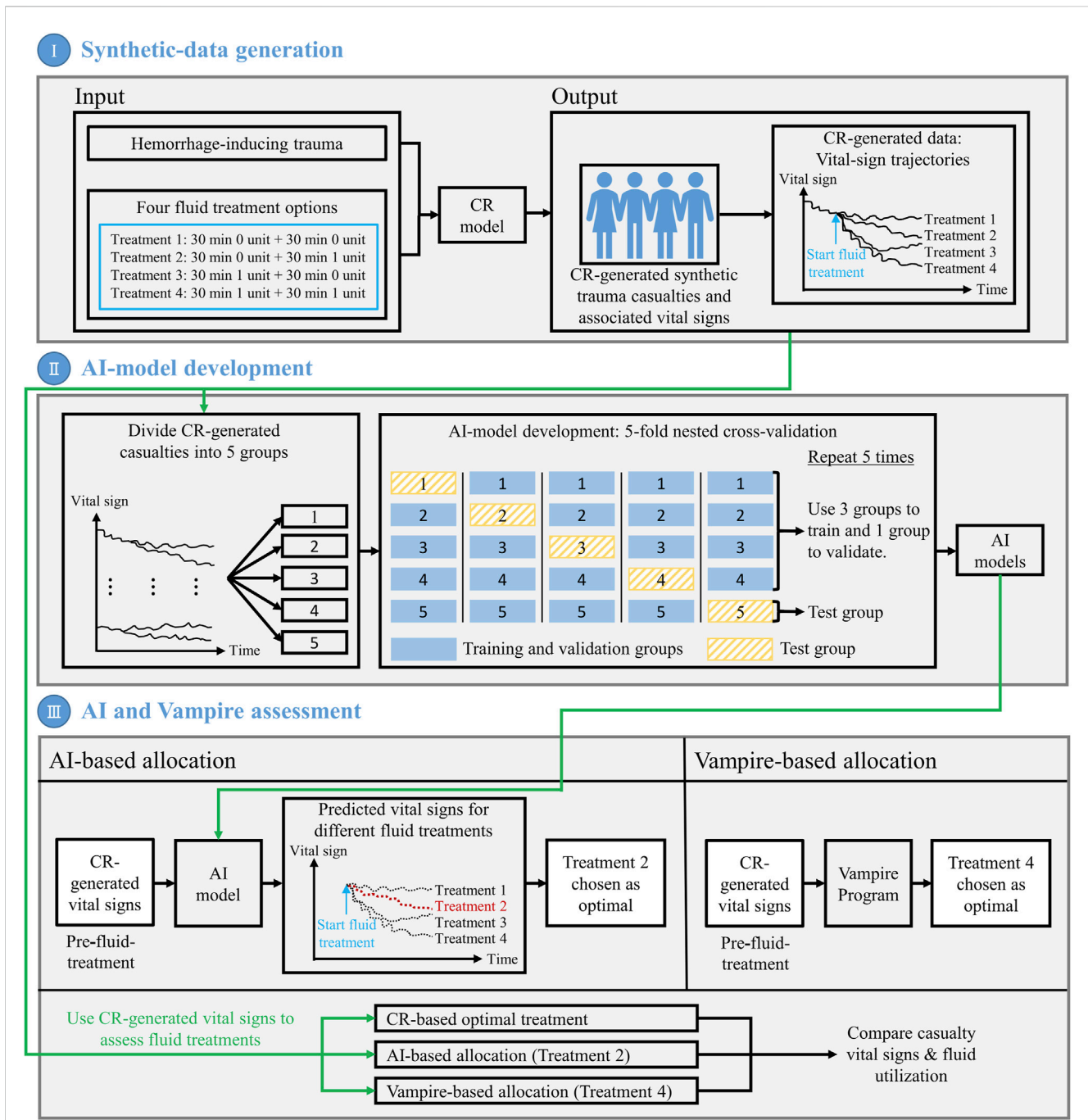


**FIGURE 1** Outline of the methodology used to develop and assess the artificial intelligence (AI) algorithm for personalized resource allocation of hemorrhage casualties. I) Synthetic-data generation: Use the cardio-respiratory (CR) model to perform simulations and generate synthetic trauma casualties with associated vital-sign trajectories, for a given hemorrhage-inducing trauma condition and each of four fluid treatment options. II) AI-model development: Using the CR-generated synthetic data, perform a 5-fold nested cross-validation to develop AI models that use 10 min of pre-fluid-treatment vital signs to predict vital signs 60 min into the future after fluid treatment. III) AI and Vampire assessment: Use the CR-generated vital-sign data to compare the outcomes in terms of the number of restored casualties to a “safe” physiological state and the amount of fluid utilization for the optimal fluid treatments allocated by the AI model and the Vampire Program as well as the CR-based optimal fluid treatment.

such that, by using 10 min of pre-fluid-treatment vital-sign data, they could predict the vital sign outcomes 60 min into the future for each of the four fluid treatments.

III) *AI and Vampire assessment.* As a final step, we assessed the performances of the AI model and the Vampire Program (Voller et al., 2021) in their ability to optimize fluid allocation

in trauma casualties in the test group. To determine the AI-based allocation, we provided the pre-fluid-treatment vital signs to the AI model, and used it to predict the vital-sign outcomes for each of the four fluid treatments. We used these predictions to choose the treatment (e.g., Treatment 2) that would lead to an optimal casualty outcome. To determine the

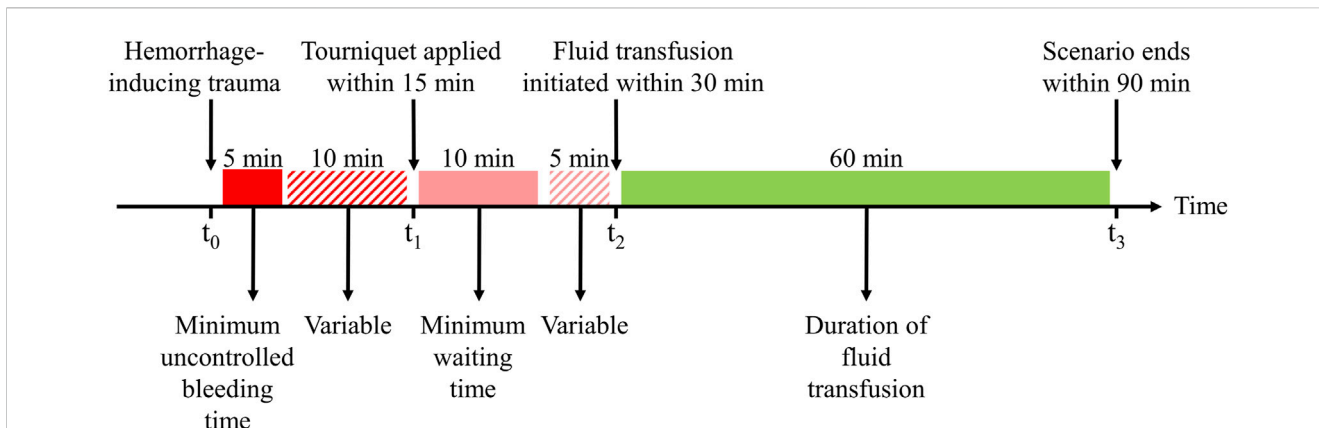


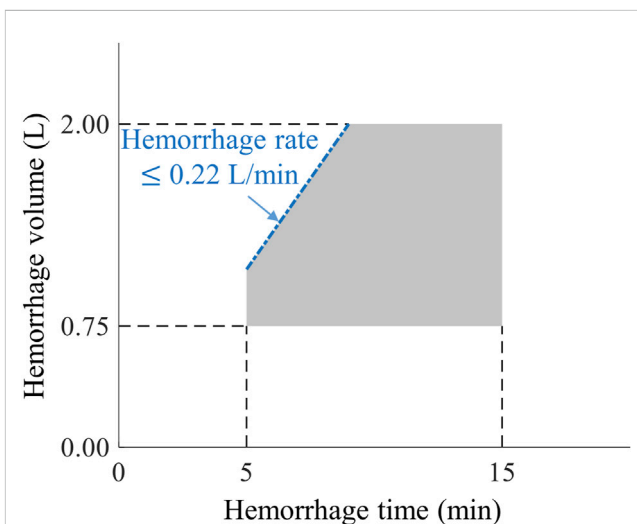
**FIGURE 2** Events and time intervals used to create different scenarios representing an initial hemorrhage-inducing trauma, tourniquet application, and subsequent fluid resuscitation treatment. The injury at  $t_0$  is followed by a period of uncontrolled bleeding for a minimum of 5 min, after which a tourniquet is applied within a 10-min interval, i.e., from 5 to 15 min after the injury. The tourniquet application at  $t_1$  stops the bleeding, the fluid transfusion at  $t_2$  is initiated at a time interval 10–15 min after  $t_1$ , and the transfusion continues for another 60 min until  $t_3$ . Different scenarios sample different time intervals between  $t_0$  and  $t_1$  to apply a tourniquet and between  $t_1$  and  $t_2$  to start the transfusion, with blood transfusion starting between 15 and 30 min after the traumatic event. The maximum transfusion time is fixed at 60 min.

Vampire-based allocation, we used its protocol to choose an optimal fluid treatment (e.g., Treatment 4) based on the pre-fluid-treatment vital signs. Finally, using the CR-generated vital-sign data, we compared the outcomes in terms of the number of restored casualties to a “safe” physiological state and the amount of fluid utilization for the optimal treatments chosen by the AI- and Vampire-based allocations as well as the “true” optimal treatment based on the CR-generated data. We repeated this procedure for each trauma casualty in each of the five test groups, using the corresponding AI model.

### Generation of hemorrhage and treatment scenarios

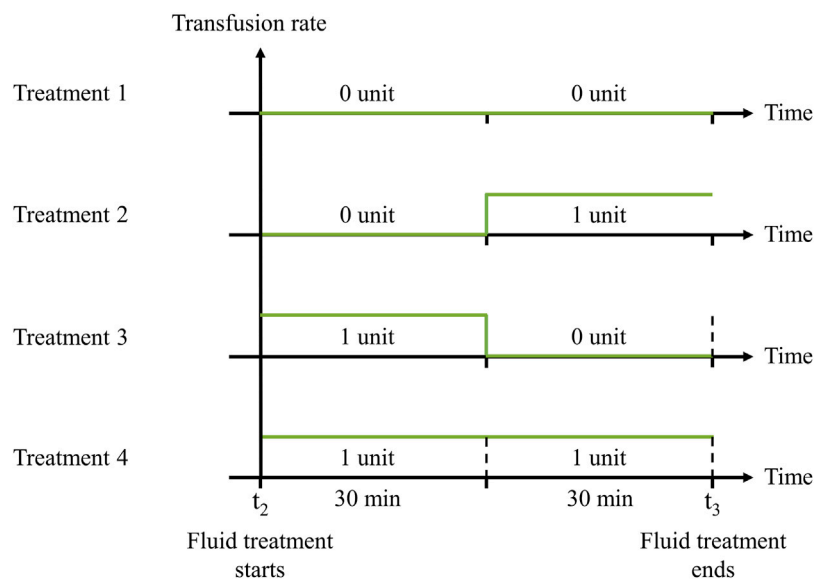
To generate synthetic vital-sign data for this study, we created variable sets of hemorrhage and treatment scenarios within defined injury, time, and fluid resuscitation limits. We created casualties corresponding to Class II and III hemorrhage (Schwartz and Holcomb, 2017), followed by a combination of tourniquet application and fluid transfusions commensurate with pre-hospital treatments documented in recent combat casualty care guidelines (Voller et al., 2021). The terms “bleeding” and “hemorrhage” with respect to the CR model correspond to a loss of fluid at a specific fixed rate for a specific length of time; to stop the bleeding, a “tourniquet” can be applied, corresponding to the bleeding rate set to zero in the CR model. This simplified hemorrhage case parallels extremity bleeding that can be controlled via the application of a tourniquet.

Figure 2 outlines the events and actions modeled in this work, i.e., the initial hemorrhage-inducing trauma occurs at  $t_0$ , followed by the application of a tourniquet to stop compressible bleeding at  $t_1$ , initiation of fluid resuscitation at  $t_2$ , and completion of the scenario at  $t_3$ . We then used a combination of fixed and variable time intervals for treatment of combat casualties in a pre-hospital setting (Voller et al.,



**FIGURE 3** The range of bleeding times and blood-volume losses used to create different hemorrhage scenarios. The pentagon-shaped area defines the range of bleeding parameters used to create Class II and III hemorrhage cases (Schwartz and Holcomb, 2017) for this study, compatible with bleeding times of 5–15 min and blood-volume losses of 0.75–2.00 L. The blue dash-dotted edge of the pentagon represents the 0.22 L/min maximum rate of hemorrhage for these scenarios.

2021). To generate moderate (Class II) and severe (Class III) hemorrhage cases that induce noticeable changes in vital signs, we introduced a period of 5 min of uncontrolled bleeding followed by a variable period of 0–10 min before application of a tourniquet. This is compatible with the reported average pre-hospital tourniquet application time in recent conflicts (Kragh et al., 2009). In the CR model, tourniquet application corresponds to completely stopping further fluid loss. Hence, for each simulated scenario, the rate of fluid loss was based on the total volume of blood loss and the time up to tourniquet application. Figure 3 shows the range of possible blood-



**FIGURE 4**  
Transfusion rates of four fluid treatment options. 1) 30 min 0 unit + 30 min 0 unit; 2) 30 min 0 unit + 30 min 1 unit; 3) 30 min 1 unit + 30 min 0 unit; or 4) 30 min 1 unit + 30 min 1 unit. The fluid treatment starts at  $t_2$  and continues for 60 min until  $t_3$ .

volume loss and bleeding time combinations that limit hemorrhage rates to the highest reported rate of 0.22 L/min (Herff et al., 2008; Soller et al., 2014; Kauvar et al., 2019).

Tourniquet application ( $t_1$ ) occurs within a maximum time of 15 min after the onset of hemorrhage, corresponding to no further fluid loss in the CR model. Subsequently, fluid transfusion is initiated at  $t_2$ , which occurs within a variable time interval of 10–15 min after  $t_1$  (Figure 2). We chose this specific time interval based on two primary considerations: 1) to ensure that the AI model had a minimum of 10 min of vital-sign data to learn the casualty's physiological state to generate personalized predictions and 2) to adhere to the military guideline that recommends the initiation of fluid resuscitation within 30 min of the hemorrhagic event (Shackelford et al., 2021).

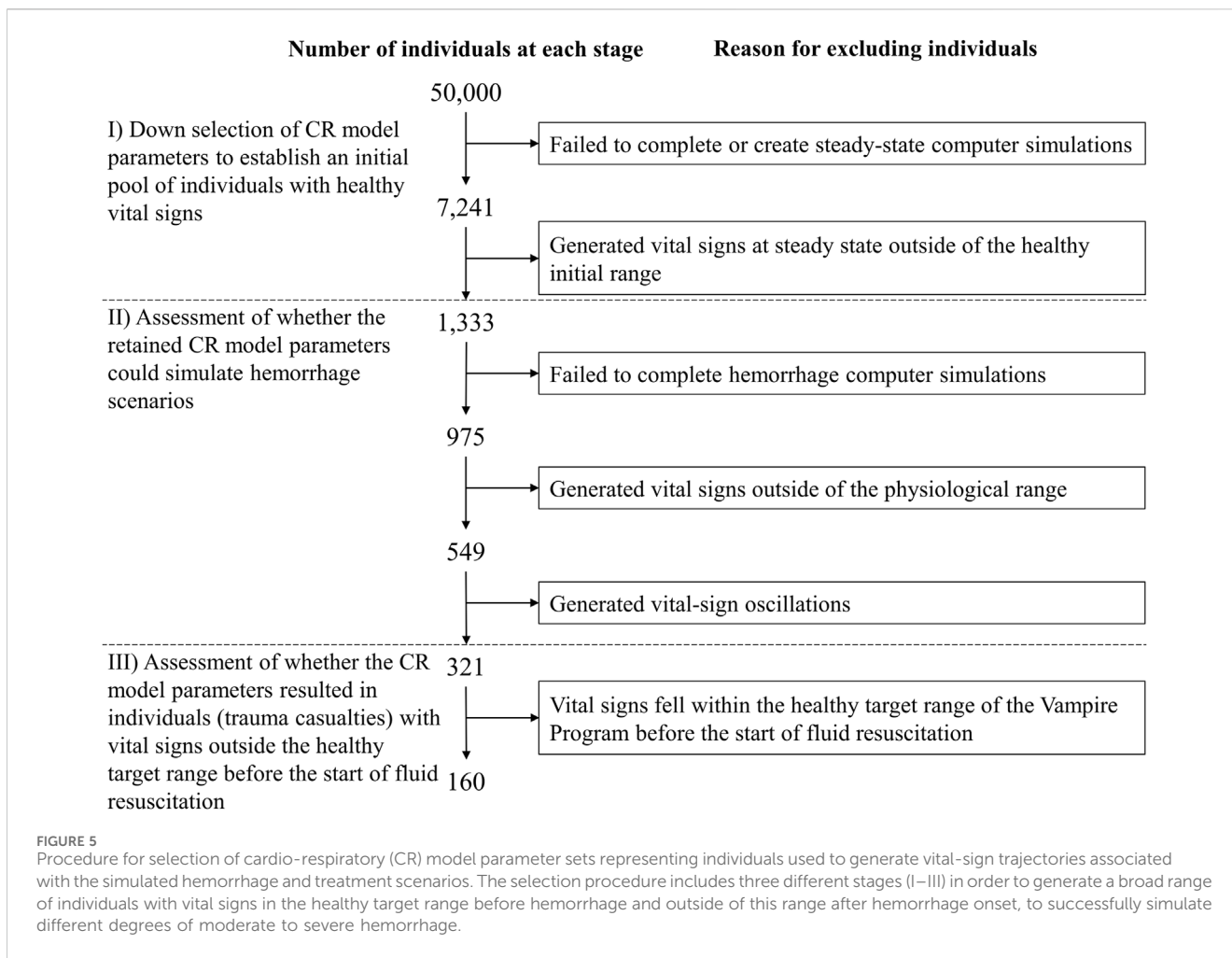
Taking into consideration that no more than 2 units of whole blood are generally administered within 60 min, with each unit containing an average volume of 0.55 L (Voller et al., 2021), we designed four distinct treatment options: 0 units for the entire 60 min; 0 units for the initial 30 min and 1 unit for the final 30 min; 1 unit for the initial 30 min and 0 units for the final 30 min; or 2 units sequentially administered in two 30-min intervals (Figure 4). For simplicity, we assumed a constant transfusion rate of 1.10 L/h. Finally, we assessed the status of the vital signs at  $t_3$ , which occurs no more than 90 min after the onset of hemorrhage.

## Generation of synthetic data

We followed a three-stage procedure to select appropriate parameter sets for generating synthetic vital-sign time-course data with the CR model, corresponding to the scenarios depicted in Figure 2 and the range of hemorrhage parameters (volume, time, and rate) defined in Figure 3. We used this process to generate a

broad range of parameter sets initially representing healthy individuals with varying initial vital-sign values that could be successfully simulated with different degrees of moderate to severe hemorrhage within the constraints discussed above. Figure 5 outlines the three stages described below.

- I) *Down selection of CR model parameters to establish an initial pool of individuals with healthy vital signs.* We used the Latin hypercube sampling method (Helton and Davis, 2003) to generate 50,000 unique model parameter sets, each representing a unique individual, by randomly sampling the 74 CR model parameter values within  $\pm 70\%$  of their nominal values. Then, we selected minimum and maximum HR values to define a “healthy” initial range, i.e., HR values higher than 60 beats/min (bradycardia) (Ou et al., 2016) and lower than 100 beats/min, as used in the Vampire Program (Voller et al., 2021). Similarly, we defined the healthy initial range for SBP as values lower than 140 mmHg (hypertension) (Gupta, 2004) and higher than 100 mmHg, as used in the Vampire Program. We only retained parameter sets with resulting vital signs in the healthy initial range.
- II) *Assessment of whether the retained CR model parameters could simulate hemorrhage scenarios.* We tested whether the selected parameter sets, where each parameter set represents one individual, could simulate the five bleeding scenarios defined by the five vertices of the pentagon-shaped area in Figure 3, which describe the outer limits of blood-volume losses and bleeding times. We applied these five scenarios and excluded parameter sets that 1) failed to complete hemorrhage simulations; 2) resulted in vital signs outside of the physiological range ( $40 \leq \text{HR} \leq 200$  beats/min and  $40 \leq \text{SBP} \leq 260$  mmHg), according to the ranges of vital-sign monitors (Mazoteras-Pardo et al., 2022; Peprah et al., 2023); or 3) generated vital-sign oscillations.



III) *Assessment of whether the CR model parameters resulted in a final pool of  $N_F$  individuals (trauma casualties) with vital signs outside of the “healthy” target range before the start of fluid resuscitation ( $t_2$ ).* Specifically, we aimed to eliminate casualties who fell within the healthy target range of the Vampire Program [ $HR \leq 100$  beats/min and  $SBP \geq 100$  mmHg (Voller et al., 2021)] at  $t_2$ , because they would not require fluid resuscitation based on the Vampire Program. Finally, we applied all four treatment options (0 units, 1 unit for the initial 30 min, 1 unit for the final 30 min, and 2 units) to each of the final pool of  $N_F$  casualties resulting in  $4N_F$  trajectories for the development of the AI model.

### Structure of the AI model

To predict how trauma casualties would respond to fluid resuscitation, we developed a recurrent neural network model, namely, a gated recurrent unit (GRU) model (Cho et al., 2014), to predict the time-series evolution of HR and SBP. Figure 6 shows the overall architecture of the model, where unlike conventional feedforward networks that process each input independently, the GRU incorporates a “memory” mechanism that enables it to learn

from a time series of inputs and update its hidden states accordingly. This functionality allows the model to capture the temporal dynamics inherent in vital signs.

At each time step  $t$ , the GRU receives three inputs: the fluid infusion rate [ $u_f(t)$ ], HR [ $HR(t)$ ], and SBP [ $SBP(t)$ ]. Consequently, it produces two outputs: the predicted HR [ $\widehat{HR}(t+1)$ ] and SBP [ $\widehat{SBP}(t+1)$ ] for the next time step (1 min in our case). The model architecture includes two feedforward layers and a GRU layer. To make personalized predictions, the GRU utilizes “measured” vital-sign data generated by the CR model from the preceding 10 min immediately before  $t_2$  (i.e., from  $t_2-10$  to  $t_2$ ), as defined in Figure 2, to update its hidden states. Starting at  $t_2$ , the GRU continuously predicts  $\widehat{HR}(t+1)$  and  $\widehat{SBP}(t+1)$  for each subsequent minute by using  $u_f(t)$  and the fed back values of  $\widehat{HR}(t)$  and  $\widehat{SBP}(t)$  until the scenario is completed at  $t_3$ . Ultimately, we utilized the final predicted values  $\widehat{HR}$  and  $\widehat{SBP}$  at  $t_3$  to evaluate the treatment outcomes, thus providing insight into the efficacy of the applied intervention at  $t_2$ .

### Development (training) of the AI model

The objective of the AI model is to use 10 min of vital-sign data before treatment of each casualty to predict the outcome of the corresponding treatment option 60 min into the future. We

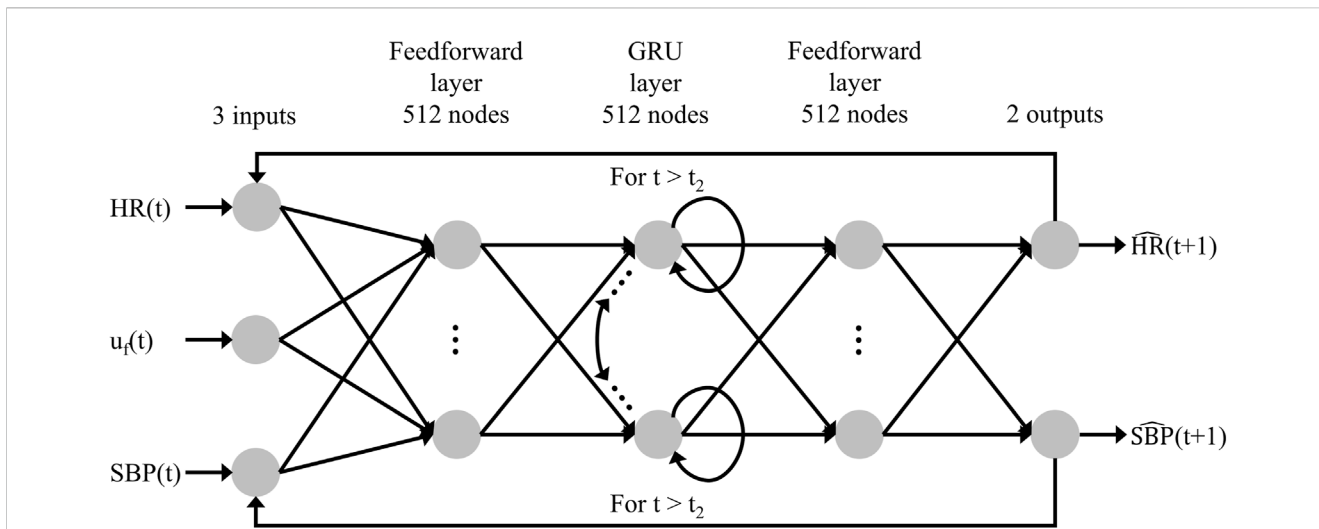


**FIGURE 6** Structure of the recurrent neural network AI model. The model’s inputs are the fluid infusion rate [ $u_f(t)$ ], heart rate [ $HR(t)$ ], and systolic blood pressure [ $SBP(t)$ ] at time  $t$ , and the outputs consist of the predicted heart rate [ $\widehat{HR}(t+1)$ ] and the predicted systolic blood pressure [ $\widehat{SBP}(t+1)$ ] for the subsequent minute. The model architecture includes two feedforward layers and a gated recurrent unit (GRU) layer, each with 512 nodes.

used the CR-generated vital signs and the corresponding fluid treatments to develop the AI model. To develop the AI model, we divided the cohort of  $N_F$  simulated trauma casualties into five groups of  $N_F/5$  casualties each and performed a 5-fold nested cross-validation procedure (Parvande et al., 2020), which simultaneously optimized the weights and hyperparameters of the model and assessed its performance. During the cross-validation procedure, we iteratively utilized three groups as the training set, one group as the validation set, and one group as the test set. Here, we trained the model with the aim of minimizing the sum of the normalized prediction error  $\epsilon$  of vital signs (HR and SBP) over the 60-min duration of fluid resuscitation, as defined by Eq. 1 below:

$$\epsilon = \sum_{t=1}^{60} \left\{ \left[ \frac{\widehat{HR}(t) - HR(t)}{150} \right]^2 + \left[ \frac{\widehat{SBP}(t) - SBP(t)}{110} \right]^2 \right\} / 60 \tag{1}$$

where  $t$  denotes a time index;  $HR(t)$  and  $SBP(t)$  denote “measured” vital signs generated by the CR model;  $\widehat{HR}(t)$  and  $\widehat{SBP}(t)$  represent the predicted HR and SBP at time  $t$ , respectively; and 150 and 110 represent normalization factors indicative of the ranges observed during the CR-model simulations. To quantitatively evaluate the AI model, we also computed the root mean square errors (RMSEs) between the AI-model predictions and the CR-generated data over 60 min of fluid transfusion for HR ( $\delta_h$ ) and SBP ( $\delta_s$ ) of the training, validation, and test sets, as defined by Eq. 2a and Eq. 2b below:

$$\delta_h = \sum_{t=1}^{60} \left[ \widehat{HR}(t) - HR(t) \right]^2 / 60 \tag{2a}$$

$$\delta_s = \sum_{t=1}^{60} \left[ \widehat{SBP}(t) - SBP(t) \right]^2 / 60 \tag{2b}$$

For details on the development of the AI model, we direct the reader to [Supplementary Text S1](#).

### Fluid allocation

We used the AI model to optimize fluid allocation and evaluated its performance by comparing it with the Vampire Program, a DoD guideline used to guide fluid resuscitation based on HR, SBP, and the presence of amputation. However, because the CR model only predicts vital signs, our analysis focused solely on HR and SBP. For the sake of simplicity, we modified the Vampire Program into a two-step process for our study: 1) prior to fluid resuscitation, if the vital signs of the casualty were not within the healthy target range [ $HR \leq 100$  beats/min and  $SBP \geq 100$  mmHg], we initiated transfusion with 1 unit of fluid for 30 min and 2) after the initial 30 min, we administered an additional unit of fluid if the CR-model-simulated vital signs continued to fall outside of the healthy target range.

Similarly, the developed AI-based fluid allocation strategy also consisted of a two-step process: 1) before initiating fluid resuscitation, we employed the AI model trained on 10 min of data to predict the outcome of the casualty at 60 min for each of the four treatment options and selected the one that used the least amount of fluids to restore the casualty’s vital signs to the healthy target range. Then, we used the CR-generated data to obtain the outcome of the selected transfusion for the initial 30 min and 2) after the 30 min, we used the available 40 min (10 + 30 min) of CR-model-simulated vital signs to update the AI model and predict the outcome at 60 min for each of two treatment options (0 or 1 unit for the final 30 min). Similarly, we selected the treatment that used the least amount of fluids to restore the casualty. When allocating fluids for a casualty within one of the five groups of  $N_F/5$  casualties, we used the AI model trained on the other four groups to predict the casualty’s vital signs. As a result, the models employed in our study do not possess any prior information regarding the casualties they are treating, ensuring a fair and unbiased allocation process. Moreover, to achieve the maximum number of casualties restored to the healthy target range with the given available fluid units, an

optimal allocation strategy should refrain from administering fluids to casualties who do not require them or who cannot be restored to the healthy target range even with 2 units. Instead, the method should prioritize administering fluids to casualties in need of 1 unit, followed by those in need of 2 units.

To perform a side-by-side comparison between the AI- and Vampire-based allocation methods, we conducted three different analyses. *Analysis 1* served as a simple demonstration of the advantages offered by the AI allocation method, while the subsequent two analyses provided deeper insights into the relative performance and effectiveness of the two allocation methods under diverse scenarios.

*Analysis 1.* We employed the two methods to allocate fluids to one casualty and compared the number of used fluid units to restore the casualty to the healthy vital-sign target range.

*Analysis 2.* We expanded our evaluation by allocating varying units of fluids to  $N_F/5$  casualties within each group, employing both allocation methods. We first compared the number of casualties restored to the healthy target range for each of the two allocation methods as well as the CR-based allocation method, which provided an upper bound of the maximum number of possible restored casualties. Regarding the CR-based allocation method, we simply used the CR-generated data to obtain the outcomes at 60 min for all four treatments and selected the one that used the least amount of fluids to restore the casualty's vital signs to the healthy target range. Similar to the AI-based allocation method, this method also prioritized administering fluids to casualties in need of 1 unit, followed by those in need of 2 units. Next, we compared the excessive use of fluids in the AI- and Vampire-based allocation methods (the number of fluid units used more than required based on the CR model).

*Analysis 3.* We explored the performance of the two allocation methods in a scenario involving the allocation of different units of fluids to varying numbers of casualties. To achieve this, we divided the  $N_F/5$  casualties of each group into different group configurations, including two groups of  $N_F/10$  casualties, four groups of  $N_F/20$  casualties, and eight groups of  $N_F/40$  casualties. Subsequently, we utilized both the AI- and Vampire-based allocation methods to distribute fluids to each group. We specifically examined the fraction of casualties restored to vital signs within the healthy target range using the AI-based method compared to the Vampire-based method. Additionally, we computed the relative ratio  $R$  of fluid-utilization efficiencies between the two methods, as defined by Eq. 3 below:

$$R = (N_A/U_A)/(N_V/U_V) \quad (3)$$

where  $N_A$  and  $N_V$  denote the total number of casualties restored to the healthy target range by the AI- and Vampire-based allocations, respectively, and  $U_A$  and  $U_V$  represent the total number of units of fluid utilized by the two methods. Hence,  $R > 1.00$  indicates a greater efficiency of the AI method over the Vampire Program allocation. To prevent an "undefined" ratio  $R$ , we only evaluated  $R$  when at least 1 unit of fluid was used (i.e.,  $U_A$  and  $U_V \neq 0$  units).

## Non-compressible bleeding detection

In the analyses above, we assumed that the tourniquet applied at time  $t_1$  set the bleeding rate to zero (completely stopped all bleeding)

and that there was no non-compressible bleeding present. Here, we aimed to demonstrate the capability of the AI model to detect cases where the casualties experienced non-compressible bleeding. As hemorrhage typically leads to an increase in HR and a decrease in SBP, casualties with non-compressible bleeding are more likely to exhibit higher HR and lower SBP values (Henry, 2018). As the AI model does not account for non-compressible bleeding, the measured vital signs may deviate from the predicted values if bleeding persists. Therefore, by assessing the disparity between the measured (as predicted by the CR model, in our case) and the AI-model-predicted vital signs, it becomes possible to identify whether a casualty is still experiencing non-compressible bleeding or not.

To verify this capability, aside from the previously generated  $4N_F$  trajectories referred to as the controlled bleeding scenario, we employed the CR model to generate an additional set of simulations for the cohort of  $N_F$  casualties. We conducted the simulations using the same bleeding rate but varied the fractions of non-compressible bleeding to 10%, 20%, 30%, 40%, and 50% of the total bleeding rate. Subsequently, we applied all four treatment options to these simulated trajectories, resulting in a total of  $N_N$  completed trajectories of non-compressible bleeding.

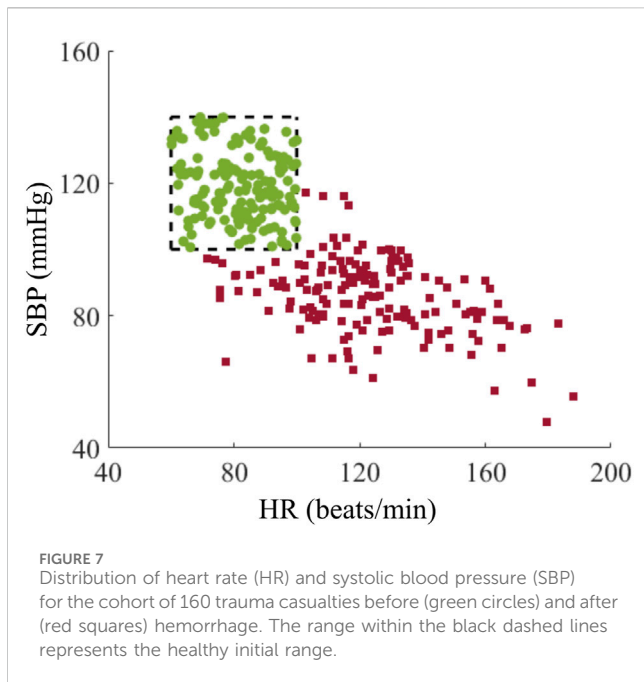
To classify the controlled and non-compressible bleeding scenarios, we utilized a support vector machine (SVM) with a linear kernel (Burgess, 1998). Given the discrepancy in the number of trajectories between the two scenarios ( $4N_F$  trajectories for controlled bleeding and  $N_N$  trajectories for non-compressible bleeding), we weighted the trajectories inversely proportional to their respective numbers for classification, ensuring that trajectories from both scenarios contributed equally to the classification analysis. After implementing the SVM algorithm on the two scenarios, we computed the classification accuracy of each scenario to assess the performance of the detection method.

## Results

### Distribution of vital signs among selected individuals

We down-selected 50,000 individuals to a pool of 160 individuals (trauma casualties) with vital signs outside of the healthy target range of the Vampire Program ( $HR \leq 100$  beats/min and  $SBP \geq 100$  mmHg) before the start of fluid resuscitation ( $t_2$ ), through three stages. Figure 5 outlines the down-selection process. In particular, Stage I) established an initial pool of 1,333 individuals with healthy vital signs; Stage II) retained 321 individuals who completed the hemorrhage scenarios; and Stage III) assigned one random bleeding scenario within the shaded region in Figure 3 to each of the remaining 321 individuals and excluded 160 individuals whose vital signs fell within the healthy target range of the Vampire Program at  $t_2$ . Finally, we randomly deselected one individual to generate a final cohort of  $N_F = 160$  trauma casualties who could be evenly divided into five groups for data generation.

To evaluate the range and variation of vital signs for the development of the AI model, we examined the distribution of their values before and after hemorrhage among the generated trauma casualties. Figure 7 shows the HR and SBP values for



each of the 160 casualties at the beginning of the injury scenario ( $t_0$ ) in [Figure 2](#), representing initial vital signs (green circles) in the healthy initial range and after hemorrhage at  $t_1$  (red squares). The initial vital signs were distributed across the entire healthy initial range, ensuring that the generated population captured a broad range of healthy baseline vital signs. In addition, the simulated hemorrhage scenarios led to an elevation in HR accompanied by a decrease in SBP, with HR values ranging between 70 and 200 beats/min and SBP values between 40 and 120 mmHg ([Figure 7](#), red squares). The upper bound of HR and the lower bound of SBP spanned the range of their respective physiological limits, reflecting the ability of the injury hemorrhage scenarios to induce significant changes in vital signs. Thus, the generated data captured a high degree of individual variability, with a range of vital-sign changes that provided a diverse set of synthetic data for the development of the AI model.

## Training, validation, and test errors of the AI model

We divided the cohort of  $N_F = 160$  trauma casualties into five groups of 32 ( $N_F/5$ ) casualties each and performed a 5-fold nested cross-validation. We first examined the three hidden layers of the recurrent neural network using 128, 256, and 512 nodes each and selected 512 nodes, as this consistently yielded the lowest average validation error  $\epsilon$  between the AI-model predictions and the synthetic data over 60 min of fluid transfusion. For detailed results of the 128- and 256-node AI models, we direct the reader to [Supplementary Figure S1](#).

[Table 1](#) shows the average and standard deviation (SD) of the RMSEs between the AI-model predictions and the synthetic data for HR and SBP. As we used the 5-fold nested cross-validation method, we trained and validated 20 ( $5 \times 4$ ) AI models. The average training RMSEs of HR ( $\delta_h$ ) and SBP ( $\delta_s$ ) over the 20 models were 3.4 (SD =

0.9) beats/min for HR and 2.5 (SD = 0.7) mmHg for SBP. Likewise, the average validation  $\delta_h$  and  $\delta_s$  were 4.2 (SD = 1.0) beats/min for HR and 2.8 (SD = 0.5) mmHg for SBP. This correspondence between the training and validation errors indicated that the AI models were not over-fitted to the training data and generalized well to unseen validation data.

Finally, the average test  $\delta_h$  and  $\delta_s$  over the five groups were 4.3 (SD = 0.7) beats/min for HR and 2.9 (SD = 0.5) mmHg for SBP. Although these errors were larger than the validation error, the absolute errors were comparable to the level of vital-sign monitor instrumental accuracy, indicating that the AI model captured changes in HR and SBP associated with fluid resuscitation treatment of a broad range of hemorrhage scenarios in a population of diverse casualties.

## Performance comparison of fluid allocation methods

We conducted three analyses to evaluate the effectiveness of fluid allocations based on the AI predictions and the Vampire Program. Given that the CR model provides the ground truth for changes in vital signs upon hemorrhage as well as treatment, we compared both allocation methods to the CR model and assessed the relative performance of each method.

In *Analysis 1*, we examined fluid allocation methods using one casualty, which like all simulated casualties had vital signs at time  $t_2$  outside of the healthy target range of the Vampire Program ([Figure 8](#)). We selected this case to highlight one possible advantage of the AI-based method, where the best fluid allocation to restore the casualty to the healthy target range according to the CR model was by giving the casualty 0 units of fluid because tourniquet application alone at time  $t_1$  was sufficient. [Figure 8](#) shows that at  $t_2$  the casualty's HR fell inside the healthy target range ([Figure 8A](#)) while the SBP did not ([Figure 8B](#)). Consequently, the Vampire Program guideline initially recommended transfusing 1 unit of fluid for the initial 30-min period. Following this period, the vital signs returned to the healthy target range ([Figure 8](#)) and the guideline recommended discontinuing the resuscitation. In contrast, the allocation choice using the AI model was based on initially predicting the outcomes of all four treatment options for the casualty. Thus, the AI model correctly predicted that all four treatment options would result in outcomes within the healthy target range and, hence, no fluid was required for this casualty.

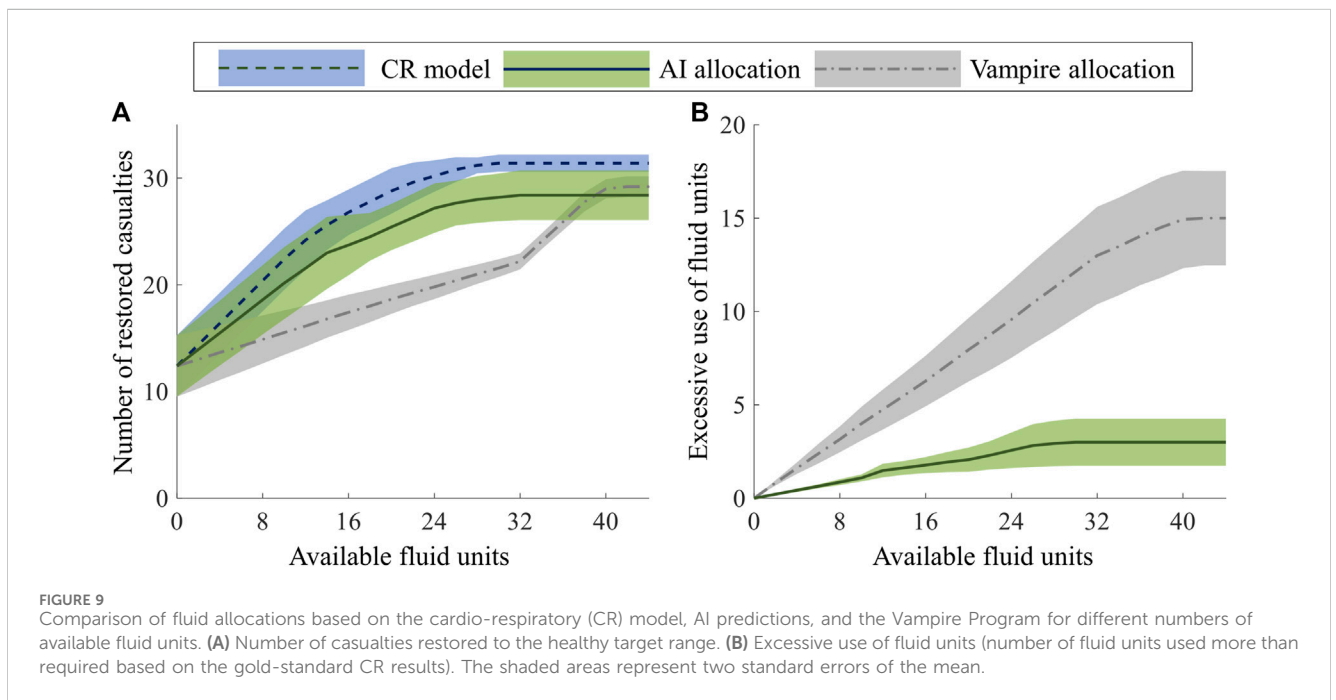
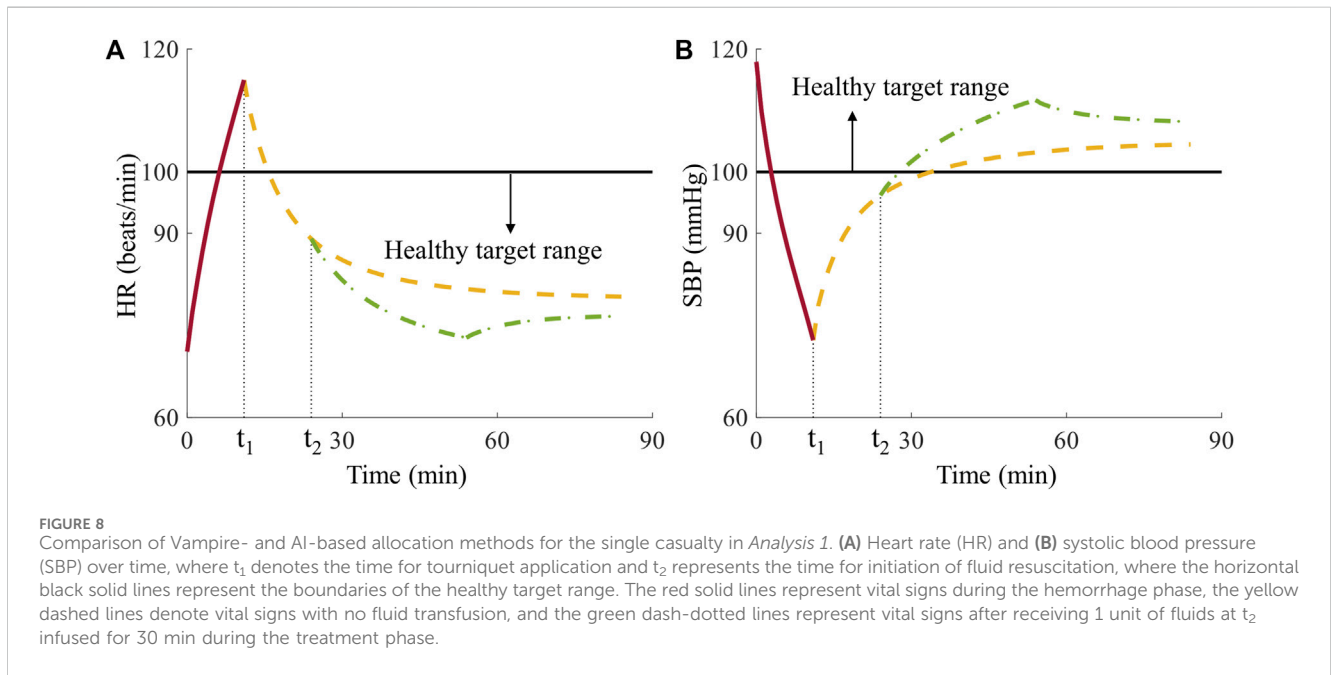
The ability of the AI-based allocation method to choose the optimal allocation strategy at the outset and ignore fixed vital-sign guidelines for fluid resuscitation allowed us to correctly transfuse 0 units of fluid to the casualty and return it to a healthy vital-sign state, while saving fluids. The predicted upfront knowledge of treatment outcomes provided the AI-based allocation a clear advantage in this case. However, the AI-based allocation method does not always outperform the Vampire Program because the model-predicted vital signs have small errors when compared to the synthetic data generated by the CR model.

In *Analysis 2*, we used a fixed number of casualties ( $N_F/5 = 32$ ) and introduced a varying number of available fluid units (0–42) for resuscitation. We compared 1) the total number of casualties

**TABLE 1** Training, validation, and test root mean square error (RMSE) between the AI-model predictions and the synthetic data generated by the cardio-respiratory model over 60 min of fluid transfusion for heart rate (HR) and systolic blood pressure (SBP).

HR RMSE ( $\delta_n$ ) (beats/min)			SBP RMSE ( $\delta_s$ ) (mmHg)		
Training (N = 20)	Validation (N = 20)	Test (N = 5)	Training (N = 20)	Validation (N = 20)	Test (N = 5)
3.4 (0.9)	4.2 (1.0)	4.3 (0.7)	2.5 (0.7)	2.8 (0.5)	2.9 (0.5)

Data are presented as mean (standard deviation). N represents the number of AI models.



restored to the healthy target range by the two allocation methods compared to the CR model and 2) the excessive recommendation and use of fluids generated by the allocation methods. To make a statistical comparison, we used the average results derived from the five groups, each made up of 32 casualties.

Figure 9A shows the number of restored casualties for the allocation methods based on the CR model (dashed line, blue shaded area), AI predictions (solid line, green shaded area), and the Vampire Program (dash-dotted line, gray shaded area). The lines and shaded areas represent the mean and two standard errors (SEs) of the mean. On average across the five groups, 12.4 casualties (2 SE = 2.9) were restored to the healthy target range without any fluid administration. As we increased the number of available fluid units for resuscitation, the average number of restored casualties rose. For the CR model (our gold standard), the average number increased at a rate of 1.0 casualty/unit until we administered 10 units, resulting in 22.4 (2 SE = 2.9) casualties restored to the healthy target range. Subsequently, the rate decreased to 0.7 casualties/unit until 16 units, leading to an average of 26.8 (2 SE = 2.1) restored casualties. Further increments in fluid units resulted in a decline in the rate to 0.5 casualties/unit until 20 units, with an average of 28.8 (2 SE = 1.9) restored casualties. Beyond 20 units, the rate continued to decrease, eventually stabilizing at 31.4 (2 SE = 0.8) restored casualties with 30 units. In contrast, the AI-based allocation restored fewer casualties compared to the CR baseline for any given number of fluid units. This was attributed to errors in the AI-model predictions and the resulting sub-optimal fluid allocation compared to the CR model. The average number of casualties restored increased at a rate of 0.8 casualties/unit until 14 units, resulting in 23.0 (2 SE = 3.4) restored casualties. Then, the rate decreased to 0.4 casualties/unit until 24 units, with an average of 27.2 (2 SE = 2.3) restored casualties. At the saturation point of 32 units, the average number of restored casualties stabilized at 28.4 (2 SE = 2.3). Comparatively, the Vampire-based allocation restored fewer casualties than the AI-based allocation. The difference was consistently larger in resource-limited conditions where the number of units was below 32. The average number of restored casualties increased only at a rate of 0.3 casualties/unit until 32 units, resulting in 22.2 (2 SE = 0.7) casualties in the healthy target range. Subsequently, the rate sharply increased to 0.9 casualties/unit until 40 units, yielding an average of 29.0 (2 SE = 0.9) restored casualties. Beyond this point, the rate became negligible, and the average number of restored casualties stabilized at 29.2 (2 SE = 1.0) up to the maximum of 42 units used for resuscitation.

Figure 9B shows the excessive use of fluids for the two allocation methods compared to the true minimum number based on the CR model. The excessive use of fluid units increased as the number of available fluid units increased, i.e., the inefficiency increased with increasing availability of fluids. For the AI-based allocation, the average excessive use of fluid units increased roughly at a rate of 0.1 per available fluid units. It peaked at 3.0 (2 SE = 1.3) units with 30 units of available fluid and saturated at this level. Comparatively, the Vampire-based allocation exhibited a much larger excessive use of fluid units, which increased at a rate of 0.4 per available fluid units until 32 units, resulting in an average of 13.0 (2 SE = 2.6) units of excessive fluid. Upon reaching 42 units, the excessive use reached a plateau, stabilizing at an average of 15.0 (2 SE = 2.5) units.

In Analysis 3, we examined variations both in the number of available fluid units (0–42) and the number of casualties (4, 8, 16, and 32) potentially requiring fluid resuscitation. Table 2 shows the fraction of casualties restored to the healthy target range using the AI-based allocation method compared to the Vampire-based allocation. The results consistently demonstrated that the AI-based method was more efficient (fraction >1.00) in resource-limited conditions across different numbers of casualties. In the case of 32 casualties, corresponding to the data shown in Figure 9A, the fraction of casualties restored to the healthy target range increased steadily until reaching 24 units of available fluid. At this point, the fraction peaked at 1.37 (SD = 0.09), indicating that the AI-based allocation method restored 37% more casualties than the Vampire-based allocation. However, beyond this point, the fraction of restored casualties started to decrease, and the two allocation methods became comparable when a larger number of fluid units were available, resulting in a fraction of ~1.00 after 40 fluid units.

To gauge fluid-utilization efficiency, we compared the relative efficiency  $R$  in Eq. 3 (i.e., the number of casualties restored per utilized fluid unit) between the two methods.  $R$  values above 1.00 indicate that, on average, the AI-based method was more efficient than the Vampire-based method. Table 3 shows this fluid-utilization efficiency metric for variable numbers of available fluid units and hemorrhage cases potentially requiring fluid resuscitation. We observed that  $R$  ranged from 1.07 (SD = 0.01) to 2.19 (SD = 1.06), demonstrating a consistently improved fluid-utilization efficiency of the AI-based allocation method over the Vampire-based allocation. Similar to as in Table 2, the relative efficiency exhibited an increasing trend followed by a subsequent decrease, with the highest value achieved when the number of fluid units equaled the number of casualties.

## Non-compressible bleeding detection

To verify if we could detect uncontrolled non-compressible bleeding, we generated 640 ( $4N_F$ ) controlled bleeding trajectories and  $N_N = 2,069$  non-compressible bleeding trajectories. Figure 10 shows the classification results of the linear SVM in differentiating controlled *versus* non-compressible bleeding. The blue circles and red squares represent the prediction errors between the AI model and the CR model (CR minus AI) for HR and SBP at  $t_3$  for the controlled and non-compressible bleeding scenarios, respectively. As expected for the controlled bleeding scenario, the mean prediction errors for both vital signs were close to zero. Most of the prediction errors ranged from -22 to 26 beats/min for HR and from -24 to 27 mmHg for SBP (blue circles). In contrast, when non-compressible bleeding was present, it caused an increase in HR and a decrease in SBP, leading to corresponding changes in their prediction errors. The prediction errors ranged from -10 to 110 beats/min for HR and from -72 to 9 mmHg for SBP (red squares). This significant difference in the prediction errors between the two scenarios serves as a potential indicator for detecting uncontrolled non-compressible bleeding.

The blue and red shaded areas in Figure 10 represent the classified areas corresponding to the controlled and non-compressible bleeding regions, respectively, in the HR/SBP

TABLE 2 Fraction of casualties restored to healthy vital signs based on the AI-based allocation method compared to the Vampire-based allocation method.

		Available fluid units												
		0	2	4	8	12	16	20	24	28	32	36	40	44
Number of casualties	32	1.00	1.07 (0.01)	1.13 (0.02)	1.25 (0.05)	1.33 (0.07)	1.36 (0.08)	1.36 (0.07)	1.37 (0.09)	1.33 (0.11)	1.28 (0.13)	1.10 (0.10)	0.98 (0.09)	0.97 (0.08)
	16	1.00	1.15 (0.05)	1.25 (0.09)	1.37 (0.16)	1.38 (0.19)	1.31 (0.26)	1.01 (0.14)	0.98 (0.11)	a	a	a	a	a
	8	1.00	1.27 (0.15)	1.37 (0.23)	1.30 (0.30)	0.98 (0.16)	a	a	a	a	a	a	a	a
	4	1.00	1.46 (0.60)	1.33 (0.59)	0.99 (0.23)	a	a	a	a	a	a	a	a	a

Fraction >1.00 indicates that the AI-based allocation method restored a larger number of casualties than the Vampire-based allocation method. Data are presented as mean (standard deviation) of the ratios of the number of casualties restored by AI-based allocation compared to those restored by the Vampire-based allocation for different numbers of available fluid units and casualties. \*Indicates that the values are equal to the value on their left.

TABLE 3 Relative fluid-utilization efficiency R of the AI-based allocation method compared to the Vampire-based allocation, where we computed the fluid-utilization efficiency as the number of casualties restored per utilized fluid units.

		Available fluid units												
		0	2	4	8	12	16	20	24	28	32	36	40	44
Number of casualties	32	1.00	1.07 (0.01)	1.13 (0.02)	1.25 (0.05)	1.33 (0.07)	1.44 (0.14)	1.53 (0.18)	1.55 (0.20)	1.64 (0.30)	1.77 (0.36)	1.70 (0.33)	1.67 (0.32)	1.66 (0.33)
	16	1.00	1.15 (0.05)	1.25 (0.09)	1.52 (0.27)	1.66 (0.36)	1.87 (0.56)	1.76 (0.56)	1.75 (0.56)	a	a	a	a	a
	8	1.00	1.27 (0.15)	1.64 (0.40)	2.04 (0.89)	1.90 (0.92)	a	a	a	a	a	a	a	a
	4	1.00	1.75 (0.69)	2.19 (1.06)	1.93 (0.96)	a	a	a	a	a	a	a	a	a

Data are presented as mean (standard deviation) of the relative efficiency R for different numbers of available fluid units and casualties. \*Indicates that the values are equal to the value on their left.

feature space. The red dashed line between the two areas denotes the decision boundary that separates the two scenarios. Because the decision boundary is neither horizontal nor vertical, both HR and SBP are essential for accurate classification. Quantitatively, the majority of the red circles and blue squares fell within their respective regions, indicating that the SVM accurately classified the bulk of the trajectories associated with the two scenarios. Table 4 shows the quantitative classification results of monitored trajectories in the two scenarios. We obtained an accuracy of 94% for the 640 controlled bleeding trajectories and an accuracy of 92% for the non-compressible bleeding trajectories, indicating the effectiveness of the AI model in detecting the presence of uncontrolled non-compressible bleeding.

## Discussion

The development, integration, and application of AI and machine-learning methods in medical care will be critical in future military conflicts to overcome anticipated challenges associated with high casualty rates, medical evacuation delays, and prolonged field care with limited resources. At all roles of medical care, the caregiver will need to efficiently match injuries with appropriate treatments under stressful conditions and with variable resource availability.

Here, we examined the utility of a deep neural network model trained on time-series vital-sign data to predict trauma-induced hemorrhage outcomes and use this knowledge to optimize casualty treatment under resource-limited conditions.

As relevant clinical data of moderate to severe hemorrhage in the pre-hospital environment are scarce and insufficient for training AI models, the use of synthetic data is key in developing and understanding the behavior of such data-driven approaches. Hence, we used a computational cardio-respiratory response model to generate synthetic data representing the time evolution of vital signs after the onset of hemorrhage, followed by the application of a tourniquet and subsequent transfusion of resuscitation fluid. By varying the volume of blood loss and transfused fluid as well as the timing of events and model parameters, the CR model allowed us to generate a sufficiently large number of synthetic casualties that we used to train a recurrent neural network AI model. In addition, the computational CR model also served as the ground-truth physiological response for human casualties against which we compared the AI-model predictions. With these capabilities, we evaluated how AI solutions could impact assessment of hemorrhage injuries and associated treatment scenarios. In particular, we explored optimizing fluid allocations under resource-limited conditions and detecting uncontrolled non-compressible bleeding.

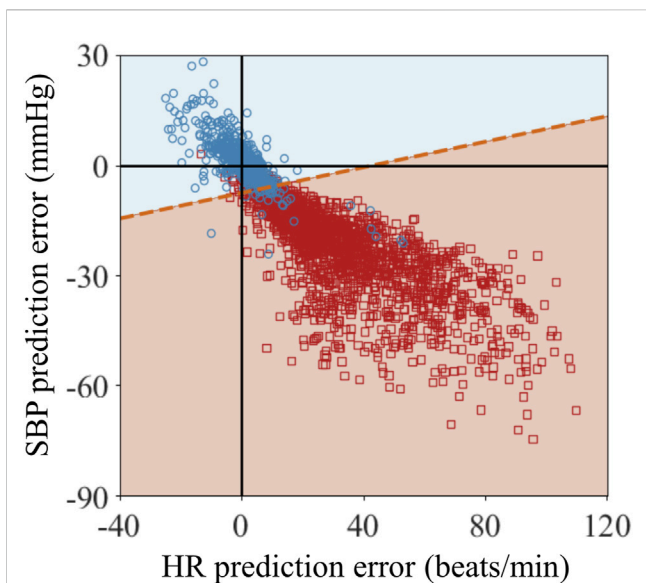


**FIGURE 10**  
 Classification results of the linear support vector machine algorithm for vital-sign trajectories at the end of fluid resuscitation at time  $t_3$  for the scenarios 1) when tourniquet application at  $t_1$  controlled bleeding and 2) when tourniquet application at  $t_1$  did not control all bleeding because there was additional non-compressible bleeding. The blue circles and red squares represent the prediction errors between the CR and AI models (CR minus AI) for heart rate (HR) and systolic blood pressure (SBP) at  $t_3$  for the two scenarios. The blue and red shaded areas represent the classified areas corresponding to controlled bleeding and non-compressible bleeding, respectively. The red dashed line between these two areas denotes the decision boundary that separates the two scenarios.

### Predictive performance of the AI model

To assess the predictive performance of the AI model, we compared its predictions with those of the ground-truth CR model results for HR and SBP. The AI model takes 10 min of initial vital-sign data after tourniquet application to make predictions of four different fluid-resuscitation treatments, ranging from no fluid up to 2 units of fluid in 60 min. The comparison of the predicted vital-sign trajectories against those of the CR data revealed low test errors ( $\delta_h$  and  $\delta_s$ ), with 4.3 beats/min (SD = 0.7) for HR and 4.1 mmHg (SD = 0.8) for SBP, indicating an overall accurate prediction of vital signs in response to different hemorrhage scenarios. The observed prediction errors were comparable to instrumental accuracy, and further attempts to

reduce these errors could potentially lead to model overfitting and, hence, compromised model generalizability. While achieving zero errors would represent an ideal scenario where the AI-based allocation method perfectly matched the CR model-based allocation, it is important to strike a balance between prediction accuracy and generalizability.

### Performance comparison of the allocation methods

With the capability to prospectively evaluate treatment options based on limited initial vital-sign data and the AI model, we can select near-optimal fluid resuscitation treatment *before* starting the fluid infusion. This allowed us to construct a predictive allocation method that considered both the available resources and the number of casualties. To assess the performance of this AI-based allocation method, we conducted three analyses to compare it with the Vampire-based allocation method. Overall, the AI-based allocations outperformed the Vampire-based allocations in all three analyses, based on different performance metrics.

### Performance of non-compressible bleeding detection

We developed a linear SVM to distinguish between controlled bleeding and uncontrolled non-compressible bleeding, achieving high classification accuracies (>90%). These results highlight the effectiveness of the SVM in accurately distinguishing between these two bleeding scenarios, even as we considered a wide range of fractions (10%–50%) of uncontrolled non-compressible bleeding out of the total bleeding rate. As expected, as the fraction of non-compressible bleeding increased, it led to a more pronounced impact on HR elevation and SBP reduction, resulting in a relatively easier detection of non-compressible bleeding. Conversely, when the fraction of non-compressible bleeding was smaller, the corresponding changes in HR and SBP were less pronounced, making the detection task more challenging.

### Limitations and assumptions

Our work has several limitations arising from both practical needs and simplifying assumptions. Importantly, the lack of vital-

**TABLE 4** Classification results of the linear support vector machine algorithm for monitored trajectories at the end of fluid resuscitation ( $t_3$ ).

Scenario	Number of trajectories	Classified as		Classification accuracy (%)
		Controlled bleeding	Non-compressible bleeding	
Controlled bleeding	640	602	38	94
Non-compressible bleeding	2,049	165	1,904	92

Classification results are shown for monitored trajectories in the following two scenarios: 1) when tourniquet application at  $t_1$  controlled any and all bleeding (Controlled bleeding) and 2) when tourniquet application at  $t_1$  did not control all bleeding because there was additional non-compressible bleeding (Non-compressible bleeding).

sign, treatment, and clinical data from actual trauma casualties precluded their use to develop a deep recurrent neural network-based AI model. Instead, we used the CR model—proven to be relatively effective in capturing the dynamics of hemorrhage and associated treatments (Voller et al., 2021)—as the ground-truth gold standard to generate vital-sign data to train the AI model and compare allocation results. Although this approach does not exactly mimic real-world complications of moderate and severe hemorrhage, the design showcases the potential of using AI techniques to capture the complex dynamics of hemorrhage and treatment scenarios. The second limitation arises from a current constraint inherent in the CR model: because it does not simulate the effects of different fluid types and only uses a generic fluid volume, it cannot account for variations in fluid types. Although it is possible to enhance the CR model to incorporate different fluid types, further work would need to be conducted to enable a more comprehensive analysis of different availabilities of fluids and their optimal allocation. This limitation is also observed in other mathematical models (Bray et al., 2019), which may allow for the selection of different fluid types but result in the exact same change in vital signs. Another limitation of our study is the consideration of treatment outcomes for only 60 min of fluid resuscitation. We made this decision to simplify the optimization process. Nonetheless, it is worth noting that our AI approach, utilizing a recurrent network model, is capable of predicting vital signs at any given future time, although prediction accuracy would decrease with an increasing prediction horizon. Nevertheless, modifying our method to account for the assessment of treatment outcomes at different time durations is a feasible option, allowing for a more detailed analysis of the effectiveness of fluid allocation strategies throughout the resuscitation process. Finally, when applying the AI model for fluid allocation, we assumed that the CR bleeding rate became zero with the application of a tourniquet, no uncontrolled non-compressible bleeding or other complications were present, and no additional medical interventions were made. While these assumptions may not accurately represent real-world scenarios, it was necessary to isolate the effects of fluid resuscitation and simplify the evaluation of the allocation process. Future research could consider incorporating uncontrolled non-compressible bleeding as well as medical countermeasures to provide a more realistic representation of trauma scenarios.

## Conclusion

We assessed the utility of a deep recurrent neural network-based AI model to capture and predict vital signs associated with hemorrhage and fluid resuscitation and investigated how to use this model in creating optimal fluid allocations to handle mass-casualty scenarios, where resources are limited. Despite the limitations of a computational model of the cardio-respiratory response, the study design allowed us to develop insights into the caveats and utility of AI-directed medical decision-making. The importance of avoiding biased data is well known in the AI field, and the presence of bias and overfitting of vital signs in AI prediction models can only be overcome by careful selection of a balanced and varied set of casualties, hemorrhage rates, and fluid resuscitation options. Simply creating more data is not necessarily beneficial; the

data must capture variable initial vital signs and represent a wide range of injury-treatment outcomes to benefit AI-model development.

Thus, our goal was not to use the CR model to generate data *per se*, but to create an application where a limited data stream (the initial 10 min of vital-sign monitoring) could be used to predict the outcome of different fluid resuscitation methods 60 min into the future. We then used knowledge of the possible outcomes to select optimal resuscitation strategies for mass-casualty scenarios under limited resource availability. Although the CR model represents a simplified hemodynamic cardiovascular response with numerous limitations, it does capture the correct coupled physiological behavior of HR and SBP variation during hemorrhage and fluid resuscitation. This allowed us to assess the potential benefits of using an allocation method that is based on personalized predictions of future outcomes *versus* a static population-based method that only uses currently available vital-sign information. The theoretical benefits of this approach include up to 46% additional casualties restored to healthy vital signs and up to a 119% efficiency increase in fluid utilization.

We further used the AI model to ascertain the error distribution of the predicted vital signs stemming from model imperfection due to training under the assumption that the bleeding rate was zero after tourniquet application. This is a valid assumption under a narrow set of conditions that exclude uncontrolled non-compressible bleeding or imperfections in the tourniquet's ability to control any and all bleeding. If we compared this scenario to CR simulation results where we manipulated the bleeding rate and set varied fractions of uncontrolled non-compressible bleeding between 10% and 50%, we could investigate the same vital-sign error distribution resulting from the use of the AI model. As the two distributions are separable, we could, in theory, use the predicted results and compare them to the ground-truth data derived from the CR model, which represent the data that could be read from a vital-sign monitor, to flag discrepancies that indicate the presence of uncontrolled non-compressible bleeding not remedied by a tourniquet application.

While this study has limitations related to the use of synthetic data under specific assumptions, the work highlights the promise of integrating neural network-based AI technologies into the field of hemorrhage detection and treatment. The simulated injury and treatment scenarios revealed prospective advantages and potential applications of AI in pre-hospital trauma care. The primary strength of this technology stems from its capacity to provide personalized outcome optimization under resource-limited conditions, such as civilian or military mass-casualty scenarios.

## Data availability statement

The raw data supporting the conclusion of this article will be made available by the authors, without undue reservation.

## Author contributions

XJ: Conceptualization, Formal Analysis, Methodology, Validation, Writing—original draft, Writing—review and editing,

Software. AF: Formal Analysis, Methodology, Validation, Writing–review and editing, Conceptualization, Software. SN: Conceptualization, Formal Analysis, Methodology, Validation, Writing–review and editing. AW: Conceptualization, Formal Analysis, Methodology, Validation, Writing–original draft, Writing–review and editing, Supervision. JR: Conceptualization, Formal Analysis, Funding acquisition, Project administration, Supervision, Validation, Writing–review and editing, Methodology.

## Funding

The author(s) declare financial support was received for the research, authorship, and/or publication of this article. The authors acknowledge support from the Combat Casualty Care Research Program of the U.S. Army Medical Research and Development Command (USAMRDC). The HJF (XJ, AF, and SN) was supported under USAMRDC Contract No. W81XWH20C0031.

## Acknowledgments

We thank Maria Kuhrmann for her editorial assistance.

## Conflict of interest

The authors declare that the research was conducted in the absence of any commercial or financial relationships that could be construed as a potential conflict of interest.

## References

- Alsalti, M., Tivay, A., Jin, X., Kramer, G. C., and Hahn, J.-O. (2022). Design and *in silico* evaluation of a closed-loop hemorrhage resuscitation algorithm with blood pressure as controlled variable. *J. Dyn. Syst. Meas. Control.* 144, 021001. doi:10.1115/1.4052312
- Avital, G., Snider, E. J., Berard, D., Vega, S. J., Hernandez Torres, S. I., Convertino, V. A., et al. (2022). Closed-loop controlled fluid administration systems: a comprehensive scoping review. *J. Pers. Med.* 12, 1168. doi:10.3390/jpm12071168
- Bray, A., Webb, J. B., Enquobahrie, A., Vicory, J., Heneghan, J., Hubal, R., et al. (2019). Pulse physiology engine: an open-source software platform for computational modeling of human medical simulation. *SN Comp. Clin. Med.* 1, 362–377. doi:10.1007/s42399-019-00053-w
- Burges, C. J. (1998). A tutorial on support vector machines for pattern recognition. *Data Min. Knowl. Discov.* 2, 121–167. doi:10.1023/A:1009715923555
- Chang, R., Cardenas, J. C., Wade, C. E., and Holcomb, J. B. (2016). Advances in the understanding of trauma-induced coagulopathy. *Blood* 128, 1043–1049. doi:10.1182/blood-2016-01-636423
- Cho, K., van Merriënboer, B., Gulcehre, C., Bahdanau, D., Bougares, F., Schwenk, H., et al. (2014). “Learning phrase representations using RNN encoder–decoder for statistical machine translation,” in *Proceedings of the 2014 conference on empirical methods in natural language processing (EMNLP)* (Doha, Qatar: Association for Computational Linguistics), 1724–1734.
- Davis, J. S., Satahoo, S. S., Butler, F. K., Dermer, H., Naranjo, D., Julien, K., et al. (2014). An analysis of prehospital deaths: who can we save? *J. Trauma Acute Care Surg.* 77, 213–218. doi:10.1097/TA.0000000000000292
- Deaton, T. G., Auten, J. D., Betzold, R., Butler, F. K., Jr., Byrne, T., Cap, A. P., et al. (2021). Fluid resuscitation in tactical combat casualty care; TCCC guidelines change 21-01. 4 November 2021. *J. Spec. Oper. Med.* 21, 126–137. doi:10.55460/JYLU-4OZ8
- Dolan, C. P., Valerio, M. S., Lee Childers, W., Goldman, S. M., and Dearth, C. L. (2021). Prolonged field care for traumatic extremity injuries: defining a role for biologically focused technologies. *NPJ Regen. Med.* 6, 6. doi:10.1038/s41536-020-00117-9
- Eastridge, B. J., Mabry, R. L., Seguin, P., Cantrell, J., Tops, T., Uribe, P., et al. (2012). Death on the battlefield (2001–2011): implications for the future of combat casualty care. *J. Trauma Acute Care Surg.* 73, S431–S437. doi:10.1097/TA.0b013e3182755dcc
- Fernandes, M., Vieira, S. M., Leite, F., Palos, C., Finkelstein, S., and Sousa, J. M. C. (2020). Clinical decision support systems for triage in the emergency department using intelligent systems: a review. *Artif. Intell. Med.* 102, 101762. doi:10.1016/j.artmed.2019.101762
- Gholami, B., Haddad, W. M., Bailey, J. M., and Muir, W. W. (2021). Closed-loop control for fluid resuscitation: recent advances and future challenges. *Front. Vet. Sci.* 8, 642440. doi:10.3389/fvets.2021.642440
- Gupta, R. (2004). Trends in hypertension epidemiology in India. *J. Hum. Hypertens.* 18, 73–78. doi:10.1038/sj.jhh.1001633
- Gurney, J. M., and Spinella, P. C. (2018). Blood transfusion management in the severely bleeding military patient. *Curr. Opin. Anaesthesiol.* 31, 207–214. doi:10.1097/ACO.0000000000000574
- Helton, J. C., and Davis, F. J. (2003). Latin hypercube sampling and the propagation of uncertainty in analyses of complex systems. *Reliab. Eng. Syst. Saf.* 81, 23–69. doi:10.1016/s0951-8320(03)00058-9
- Henry, S. (2018). ATLS 10th edition offers new insights into managing trauma patients. *Bull. Am. Coll. Surg.* 103, 15–22.
- Herff, H., Paal, P., von Goedecke, A., Lindner, K. H., Severing, A. C., and Wenzel, V. (2008). Influence of ventilation strategies on survival in severe controlled hemorrhagic shock. *Crit. Care Med.* 36, 2613–2620. doi:10.1097/CCM.0b013e31818477f0
- Hodgman, E. I., Cripps, M. W., Mina, M. J., Bulger, E. M., Schreiber, M. A., Brasel, K. J., et al. (2018). External validation of a smartphone app model to predict the need for massive transfusion using five different definitions. *J. Trauma Acute Care Surg.* 84, 397–402. doi:10.1097/TA.0000000000001756
- Jin, X., Bighamian, R., and Hahn, J. O. (2018). Development and *in silico* evaluation of a model-based closed-loop fluid resuscitation control algorithm. *IEEE Trans. Biomed. Eng.* 66, 1905–1914. doi:10.1109/TBME.2018.2880927

The author(s) declared that they were an editorial board member of Frontiers, at the time of submission. This had no impact on the peer review process and the final decision.

## Publisher’s note

All claims expressed in this article are solely those of the authors and do not necessarily represent those of their affiliated organizations, or those of the publisher, the editors and the reviewers. Any product that may be evaluated in this article, or claim that may be made by its manufacturer, is not guaranteed or endorsed by the publisher.

## Author disclaimer

The opinions and assertions contained herein are the private views of the authors and are not to be constructed as official or as reflecting the views of the U.S. Army, the U.S. Department of Defense, or The Henry M. Jackson Foundation (HJF) for the Advancement of Military Medicine, Inc. This paper has been approved for public release with unlimited distribution.

## Supplementary material

The Supplementary Material for this article can be found online at: <https://www.frontiersin.org/articles/10.3389/fphys.2024.1327948/full#supplementary-material>

- Jin, X., Laxminarayan, S., Nagaraja, S., Wallqvist, A., and Reifman, J. (2023). Development and validation of a mathematical model to simulate human cardiovascular and respiratory responses to battlefield trauma. *Int. J. Numer. Method Biomed. Eng.* 39, e3662. doi:10.1002/cnm.3662
- Kauvar, D. S., Schechtman, D. W., Thomas, S. B., Prince, M. D., De Guzman, R., Polykratis, I. A., et al. (2019). Effect of partial and complete aortic balloon occlusion on survival and shock in a swine model of uncontrolled splenic hemorrhage with delayed resuscitation. *J. Trauma Acute Care Surg.* 87, 1026–1034. doi:10.1097/TA.0000000000002439
- Kisat, M., Morrison, J. J., Hashmi, Z. G., Efron, D. T., Rasmussen, T. E., and Haider, A. H. (2013). Epidemiology and outcomes of non-compressible torso hemorrhage. *J. Surg. Res.* 184, 414–421. doi:10.1016/j.jss.2013.05.099
- Kragh, J. F., Walters, T. J., Baer, D. G., Fox, C. J., Wade, C. E., Salinas, J., et al. (2009). Survival with emergency tourniquet use to stop bleeding in major limb trauma. *Ann. Surg.* 249, 1–7. doi:10.1097/SLA.0b013e31818842ba
- Kramer, G. C., Kinsky, M. P., Prough, D. S., Salinas, J., Sondeen, J. L., Hazel-Scerbo, M. L., et al. (2008). Closed-loop control of fluid therapy for treatment of hypovolemia. *J. Trauma.* 64, S333–S341. doi:10.1097/TA.0b013e31816bf517
- Lammers, D., Marengo, C., Morte, K., Conner, J., Williams, J., Bax, T., et al. (2022). Machine learning for military trauma: novel massive transfusion predictive models in combat zones. *J. Surg. Res.* 270, 369–375. doi:10.1016/j.jss.2021.09.017
- Lesperance, R. N., Adamson, S., and Gurney, J. M. (2023). Lessons learned during prolonged care of combat casualties by a minimally manned surgical team. *Mil. Med.* 188, e1389–e1394. doi:10.1093/milmed/usab299
- Liu, N. T., Holcomb, J. B., Wade, C. E., Batchinsky, A. I., Cancio, L. C., Darrach, M. I., et al. (2014). Development and validation of a machine learning algorithm and hybrid system to predict the need for life-saving interventions in trauma patients. *Med. Biol. Eng. Comput.* 52, 193–203. doi:10.1007/s11517-013-1130-x
- Liu, S., Wright, A. P., Patterson, B. L., Wanderer, J. P., Turer, R. W., Nelson, S. D., et al. (2023). Using AI-generated suggestions from ChatGPT to optimize clinical decision support. *J. Am. Med. Inf. Assoc.* 30, 1237–1245. doi:10.1093/jamia/ocad072
- Marques, N. R., Ford, B. J., Khan, M. N., Kinsky, M., Deyo, D. J., Mileski, W. J., et al. (2017). Automated closed-loop resuscitation of multiple hemorrhages: a comparison between fuzzy logic and decision table controllers in a sheep model. *Disast. Mil. Med.* 3, 1–10. doi:10.1186/s40696-016-0029-0
- Mazoterias-Pardo, V., Gomez-Cantarino, S., Ramirez-Jimenez, M., Navarro-Flores, E., and Ugarte-Gurrutxaga, M. I. (2022). Validations of blood pressure measuring devices using recognized protocols. *J. Pers. Med.* 13, 9. doi:10.3390/jpm13010009
- Mina, M. J., Winkler, A. M., and Dente, C. J. (2013). Let technology do the work: improving prediction of massive transfusion with the aid of a smartphone application. *J. Trauma Acute Care Surg.* 75, 669–675. doi:10.1097/TA.0b013e3182a12ba6
- Ou, S. H., Tang, Y., Polli, A., Wilner, K. D., and Schnell, P. (2016). Factors associated with sinus bradycardia during crizotinib treatment: a retrospective analysis of two large-scale multinational trials (profile 1005 and 1007). *Cancer Med.* 5, 617–622. doi:10.1002/cam4.622
- Parvande, S., Yeh, H. W., Paulus, M. P., and McKinney, B. A. (2020). Consensus features nested cross-validation. *Bioinformatics* 36, 3093–3098. doi:10.1093/bioinformatics/btaa046
- Peng, H. T., Siddiqui, M. M., Rhind, S. G., Zhang, J., da Luz, L. T., and Beckett, A. (2023). Artificial intelligence and machine learning for hemorrhagic trauma care. *Mil. Med. Res.* 10, 6. doi:10.1186/s40779-023-00444-0
- Peprah, Y. A., Lee, J. Y., and Persell, S. D. (2023). Validation testing of five home blood pressure monitoring devices for the upper arm according to the ISO 81060-2:2018/AMD 1:2020 protocol. *J. Hum. Hypertens.* 37, 134–140. doi:10.1038/s41371-022-00795-6
- Raita, Y., Goto, T., Faridi, M. K., Brown, D. F. M., Camargo, C. A., Jr., and Hasegawa, K. (2019). Emergency department triage prediction of clinical outcomes using machine learning models. *Crit. Care.* 23, 64–13. doi:10.1186/s13054-019-2351-7
- Rinehart, J., Lee, C., Canales, C., Kong, A., Kain, Z., and Cannesson, M. (2013). Closed-loop fluid administration compared to anesthesiologist management for hemodynamic optimization and resuscitation during surgery: an *in vivo* study. *Anesth. Analg.* 117, 1119–1129. doi:10.1213/ANE.0b013e3182937d61
- Schwartz, D. A., and Holcomb, J. (2017). “Initial resuscitation and management of the hemodynamically unstable patient,” in *Common problems in acute care surgery*. Editors L. Moore and S. Todd (Cham: Springer), 3–15.
- Shackelford, S. A., Gurney, J. M., Taylor, A. L., Keenan, S., Corley, J. B., Cunningham, C. W., et al. (2021). Joint trauma system, defense committee on trauma, and armed services blood program consensus statement on whole blood. *Transfusion* 61, S333–S335. doi:10.1111/trf.16454
- Soller, B., Smith, C., Zou, F., Ellerby, G. E., Prince, M. D., and Sondeen, J. L. (2014). Investigation of noninvasive muscle pH and oxygen saturation during uncontrolled hemorrhage and resuscitation in swine. *Shock* 42, 44–51. doi:10.1097/SHK.0000000000000174
- Stallings, J. D., Laxminarayan, S., Yu, C., Kapela, A., Frock, A., Cap, A. P., et al. (2023). APPRAISE-HRI: an artificial intelligence algorithm for triage of hemorrhage casualties. *Shock* 60, 199–205. doi:10.1097/SHK.0000000000002166
- Voller, J., Tobin, J. M., Cap, A. P., Cunningham, C. W., Denoyer, M., Drew, B., et al. (2021). Joint trauma system clinical practice guideline (JTS CPG): prehospital blood transfusion. 30 October 2020. *J. Spec. Oper. Med.* 21, 11–21. doi:10.55460/P685-L7R7
- Walker, H. L., Ghani, S., Kuemmerli, C., Nebiker, C. A., Muller, B. P., Raptis, D. A., et al. (2023). Reliability of medical information provided by ChatGPT: assessment against clinical guidelines and patient information quality instrument. *J. Med. Internet Res.* 25, e47479. doi:10.2196/47479